

# Conjugated Polyelectrolytes—Conformation-Sensitive Optical Probes for Staining and Characterization of Amyloid Deposits

K. Peter R. Nilsson,<sup>\*[a, e]</sup> Per Hammarström,<sup>[b]</sup> Fredrik Ahlgren,<sup>[c]</sup> Anna Herland,<sup>[a]</sup> Edrun A. Schnell,<sup>[d]</sup> Mikael Lindgren,<sup>[d]</sup> Gunilla T. Westermark,<sup>[c]</sup> and Olle Inganäs<sup>[a]</sup>

*Specific markers for diseases associated with protein aggregate depositions are of great interest. Here we report the use of conjugated polyelectrolytes as conformation-sensitive optical probes for histological labeling of amyloid deposits in ex vivo tissue samples—amyloid light chains in primary systemic amyloidosis, islet amyloid polypeptide in human pancreas, and A $\beta$  amyloid in Alzheimer's disease. Under suitable conditions, these probes bind specifically to amyloid deposits, and this is seen as an orange-red emission from the polyelectrolyte. Furthermore, the probes emit*

*light of different colors when bound to different amyloid deposits or other intracellular structures. This phenomenon is most probably due to differences in the protein conformation in these structures. Hence, different protein conformations will generate geometric alterations of the bound polyelectrolyte backbone, affording different emissions from the bound probe. Conformation-sensitive probes thus provide a direct link between spectral signal and protein conformation. Finally, the probes also proved useful for ex vivo fluorescence imaging by multiphoton excitation.*

## Introduction

Proteins frequently alter their conformation as a response to different external stimuli, and the importance of conformational changes of proteins leading to pathogenic states has been well documented.<sup>[1–6]</sup> Especially under conditions that destabilize the native state, proteins can aggregate into characteristic  $\beta$  sheet-rich fibrillar assemblies, known as amyloid fibrils.<sup>[7–11]</sup> The extracellular deposition of amyloid fibrils is a hallmark of many devastating diseases, known as the amyloidoses and including Alzheimer's disease (AD) and the systemic amyloidoses. Diseases such as Huntington's disease and the prion diseases also display aggregated protein deposits with many amyloid characteristics.

Histological staining of the amyloid deposits is crucial for the diagnosis of amyloidoses. Thioflavin T or S (ThT or ThS) and Congo red are normally used as detection agents for amyloids, but these probes have some major disadvantages:<sup>[12–14]</sup> amyloids stained with Congo red demonstrate green birefringence in cross polarized light, but this standard method requires good control and experience to be reliable, whilst ThT and ThS are blue-emissive dyes, which often interfere with autofluorescence from tissue. Therefore, simple, sensitive, and versatile tools to detect the fibrillar conformations of amyloidogenic proteins are of great importance. In this regard, we have utilized fluorescent conjugated polyelectrolytes (CPs) as amyloid-specific dyes for staining of amyloid-containing tissue.

The conformational flexibility of CPs allows a direct correlation between the geometry of the chains and the resulting electronic structure and processes. This requires that the conjugated polyelectrolyte chain geometry be governed by bio-

molecules. Hence, upon complex formation between a biomolecule and a CP, conformational changes in the biomolecule should lead to different conformations of the bound polyelectrolyte backbone, and an alteration of the absorption and emission properties from the polyelectrolyte should be observable, providing a direct link between spectral signal and protein conformation. In previous studies we have shown that CPs can be used as conformation-sensitive optical probes for the


[a] Dr. K. P. R. Nilsson, A. Herland, Prof. O. Inganäs  
Biomolecular and Organic Electronics, IFM, Linköping University  
581 83 Linköping (Sweden)  
Fax: (+46) 13-28-89-69  
E-mail: petni@ifm.liu.se

[b] Prof. P. Hammarström  
Chemistry, IFM, Linköping University  
581 83 Linköping (Sweden)

[c] F. Ahlgren, Prof. G. T. Westermark  
Division of Cell Biology and Diabetes Research Centre, Linköping University  
581 83 Linköping (Sweden)

[d] E. A. Schnell, Prof. M. Lindgren  
Department of Physics  
The Norwegian University of Science and Technology  
7491 Trondheim (Norway)

[e] Dr. K. P. R. Nilsson  
Current address:  
Institute of Neuropathology, University Hospital Zürich  
8091 Zürich (Switzerland)  
Fax: (+41) 44-255-54-02  
E-mail: peter.nilssoni@usz.ch

 Supporting information for this article is available on the WWW under <http://www.chembiochem.org> or from the author.

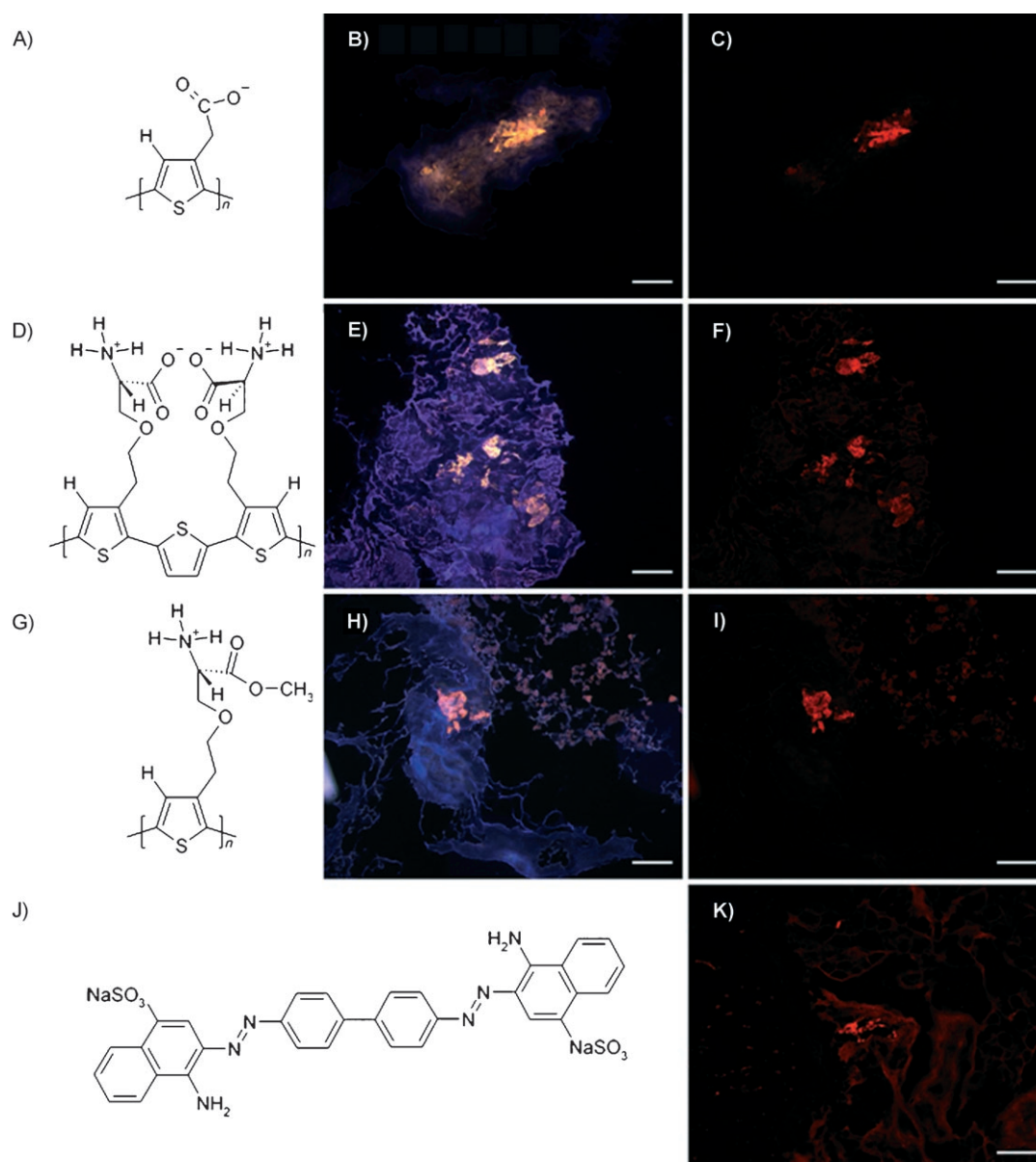


**Figure 1.** Chemical structures of different conjugated polyelectrolytes and fluorescence images of islet amyloid in human pancreas. B) and C) Tissue stained with PTAA (A;  $2.5 \mu\text{g mL}^{-1}$ ) in Na carbonate (100 mM, pH 10) for 2 h. E) and F) Tissue stained with PONT (D;  $2.5 \mu\text{g mL}^{-1}$ ) in glycine-HCl (100 mM, pH 2.5) for 2 h. H) and I) Tissue stained with POMT (G;  $2.5 \mu\text{g mL}^{-1}$ ) in Na carbonate (100 mM, pH 10) for 2 h. K) Tissue stained by Congo red (J). Images B, E, and H are multifilter images, recorded with an epifluorescence microscope through a 405/30 nm filter (LP450), a 470/40 nm filter (LP515), a 546/12 nm filter (LP590), and a  $10\times$  objective. Images C, F, I, and K were recorded with an epifluorescence microscope through a 546/12 nm filter (LP590) and a  $10\times$  objective. Scale bars (white lines) represent  $150 \mu\text{m}$ .

detection of DNA hybridization,<sup>[15]</sup> conformational changes in synthetic peptides,<sup>[16,17]</sup> and calcium-induced conformational changes in calmodulin.<sup>[18]</sup> Most recently, anionic and zwitterionic CPs were also used to monitor amyloid fibril formation *in vitro*.<sup>[19,20]</sup> The detection principle is based on conformational changes in the polyelectrolyte chains when binding to a native protein or to the same protein trapped in cross- $\beta$  sheet amyloid fibrils and is readily detected by optical absorption and emission. In this study, we have used three different CPs—polythiophene acetic acid (PTAA- $\text{Li}^+$ ), poly(3,3'-di[(S)-5-amino-5-carboxyl-3-oxapentyl]-[2,2';5',2'']-5,5''-terthiophenylene) hydrochloride (PONT), and poly(3-[(S)-5-amino-5-carboxyl-3-oxa-

pentyl]-2,5-thiophenylene) hydrochloride (POMT; Figure 1)—for staining of amyloid deposits in tissue samples. Furthermore, PTAA has been evaluated as a conformation-sensitive optical probe for use in optical imaging of tissue samples by multiphoton spectroscopy.

## Results and Discussion

At first glance, the versatility of the binding of the CPs to several biomolecules made histological staining studies appear unlikely, due to severe competition in a complex sample such as tissue. Staining with PTAA was first performed in Na phos-

phate (20 mM, pH 7.0), as these conditions have previously been used for the detection of amyloid deposits *in vitro*,<sup>[19]</sup> but with this staining protocol no specific binding to the amyloid deposits were observed and most of the tissue was stained by the PTAA (data not shown). We therefore explored a staining protocol with a more alkaline buffer solution (100 mM Na carbonate, pH 10) to elucidate selective staining conditions for PTAA. At this pH, interactions between PTAA and other molecules, such as proteins and nucleic acids, in the tissue samples should be unfavorable due to electrostatic repulsion, as most of the biomolecules and PTAA are negatively charged at pH 10. On the other hand, both the amyloid deposits and PTAA are hydrophobic and show highly repetitive structures, which should promote specific interactions between PTAA and the amyloid deposits.

PTAA (Figure 1A) was first tested for binding to islet amyloid in frozen pancreas tissues fixed in acetone or ethanol. The characteristic orange-red fluorescence of PTAA (pH 10; Figure 1) would be expected from planar polyelectrolyte chains bound to ordered amyloid fibrils.<sup>[19]</sup> Under a fluorescence microscope, binding of the probe to amyloid with PTAA dissolved in Na carbonate buffer (pH 10) revealed a strong fluorescence signal (Figure 1B and C). The polyelectrolyte emits orange-red light upon binding to the amyloid deposits, and the deposits can easily be discriminated from the rest of the tissue (blue autofluorescence). These red-shifted emission signals are very different from signals from the CPs bound to other fibrillar structures such as collagen, where the emission colors range from green to yellow,<sup>[19]</sup> so specific binding of PTAA to the amyloid deposits was achieved under these new staining conditions (100 mM Na carbonate, pH 10.0). The presence of islet amyloid in this material was also verified by Congo red staining<sup>[21,22]</sup> (Figure 1K). We observed that PTAA showed a labeling pattern identical to that seen with Congo red staining and that PTAA was at least as sensitive as Congo red in terms of labeling amyloid deposits. At this pH, the polyelectrolyte acts as an amyloid-specific dye and can be used as a probe for diagnosis of amyloid-related diseases. The specificity is possibly due to hydrophobic interactions between the polyelectrolyte and the amyloid fibril, these being stabilized through hydrogen bonds between the anionic carboxyl groups of the polyelectrolyte side chains and the amyloid fibrils. Interestingly, initial experiments with samples pretreated with formic acid have revealed that this pretreatment eliminates most of the binding of PTAA to amyloid plaques, suggesting that PTAA binds to  $\beta$ -pleated sheets, as it has been shown with other probes that formic acid disrupts the  $\beta$ -pleated structure<sup>[23]</sup> and destroys staining of amyloid plaques.<sup>[24]</sup>

A local pH change in the plaques or insufficient washing and neutralization could also be reasons for inadequate staining. To test this hypothesis, additional experiments with PTAA, using samples preincubated for 30 min with HCl (50 mM, pH 1.6) or glycine-HCl (100 mM, pH 2.5; the same buffer as used for PONT staining—see below) were performed. After removal of the acid solutions and without any washing steps, a staining solution of PTAA in Na carbonate (100 mM, pH 10) was added to the sections and the samples were incubated for

2 h. Interestingly, the staining worked perfectly in these cases and intense fluorescence was observed from PTAA bound to these plaques, so these experiments indicate that a local pH change in the plaques or insufficient washing and neutralization do not prevent adequate staining with PTAA. Instead, the explanation that formic acid treatment of tissue prevents binding of PTAA to amyloid plaques due to disruption of the  $\beta$ -pleated sheet structure is more plausible.

Amyloid staining by the zwitterionic conjugated oligoelectrolyte PONT (Figure 1D), dissolved in an acidic buffer solution (pH 2.5), also revealed an excellent fluorescent signal from the amyloid deposits (Figure 1E and F). At acidic pH, PONT binds specifically to the amyloid deposits<sup>[20]</sup> and emits red light that can easily be separated from the blue autofluorescence of the frozen tissue. At acidic pH, the zwitterionic side chains have a predominantly positive charge. Similarly to the case of PTAA, the amyloid binding specificity is most probably the result of hydrophobic interactions and hydrogen bonding between PONT and the repetitive structure of the amyloid fibrils. As PONT and most of the biomolecules in the tissue sample are positively charged at acidic pH, unspecific interactions are not seen, due to electrostatic repulsion. In some samples, however, staining of cell nuclei were observed to a certain extent. In contrast with the results seen for PTAA, initial experiments with samples pretreated with formic acid have revealed that this pretreatment does not eliminate the binding of PONT to amyloid deposits. PONT is a smaller molecule than PTAA, and initial experiments using polarization microscopy indicate that these CPs bind differently from amyloid fibrils, so alternative binding sites on the amyloid fibrils might be the reason for PONT binding to deposits pretreated with formic acid.

The cationic fluorescent polyelectrolyte POMT (Figure 1G) can also be used as an amyloid-specific dye (Figure 1H and I). If the tissue samples are stained with POMT diluted in Na carbonate (pH 10), the amyloid plaque emits red light, due to specific binding of the polyelectrolyte. The cationic amine groups can be protonated or deprotonated in water solution ( $pK_a$  of the amine group of serine = 9.2), and these groups are preferably in the unprotonated form at pH 10. The side chain of the polyelectrolyte is therefore highly hydrophobic at pH 10, which provides specific binding of POMT to the hydrophobic amyloid deposits. As the polyelectrolyte is mostly in the unprotonated form at pH 10 there is a risk that the polyelectrolyte might not form a stable solution, and a previous study<sup>[25]</sup> using higher concentrations of POMT in alkaline buffer solutions of lower ionic strength showed that the polyelectrolyte chains would aggregate. However, under the conditions used in these experiments—first dissolving the probe in deionized water and then diluting the probe to a final concentration of  $2.5 \mu\text{g mL}^{-1}$  in  $\text{Na}_2\text{CO}_3$  buffer (100 mM, pH 10)—no precipitation of the polyelectrolyte was observed during the time of staining. The staining can also be performed with buffer solutions at acidic pH (pH 2.5), at which POMT is positively charged. At low pH values a certain unspecific binding to cell nuclei was observed, probably due to electrostatic interactions between DNA and POMT. Under these conditions, however, POMT also showed good colocalization with Congo red labeling and the amyloid

plaques could easily be differentiated from the rest of the tissue.

To demonstrate further that CPs can be used for staining of amyloid deposits in tissue samples, PTAA was tested on formaldehyde-fixed, paraffin-embedded tissue material from AD patients. As shown in Figures 2 and 3, PTAA binds specifically to A $\beta$  amyloid deposits in these tissue samples and the deposits are easily distinguished from the rest of the tissue, due to red emission from the PTAA-stained amyloid. The specificity for PTAA labeling of amyloid was analyzed by comparison of staining patterns for PTAA and Congo red on serial sections (compare the amyloid-coated vascular vessels in the lower left of Figure 3F and 3A–E). A variety of amyloid deposits were revealed in the PTAA-stained AD samples: diffuse plaques (Figure 2A and B), vascular amyloid (Figure 3A–E), and solid micron-sized plaques (Figure 2D). The micron-sized plaques were scarce and only present in <5% of the brain section specimen and could represent an early stage of A $\beta$  accumulation.

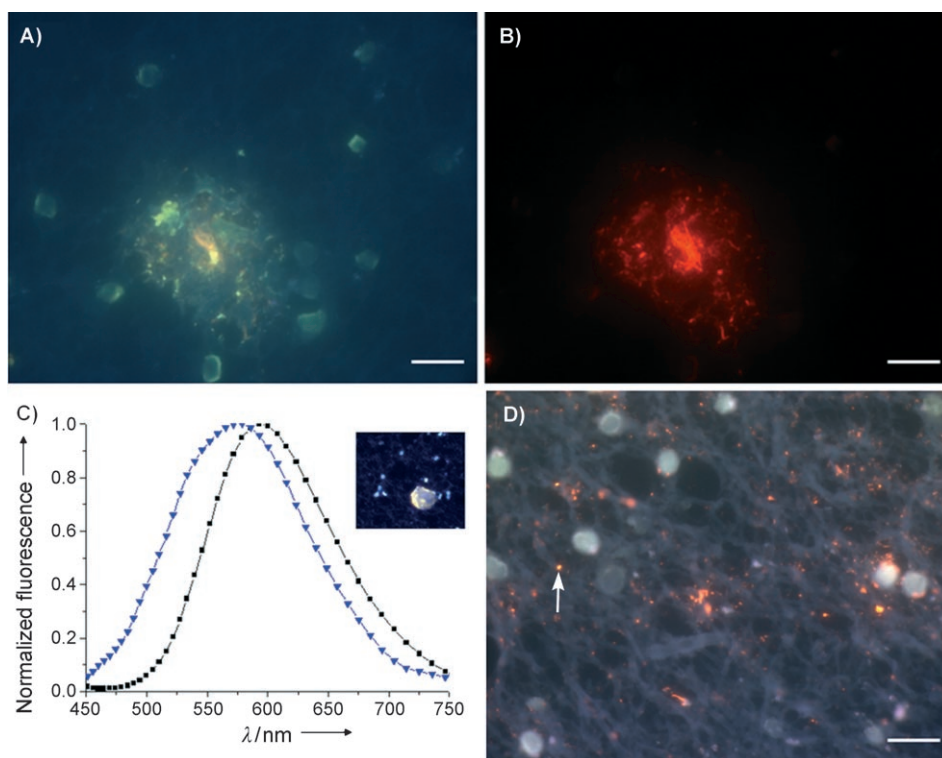


**Figure 2.** Fluorescence images and spectra of brain tissue from AD patients stained with PTAA. A) and B) Images of brain tissue containing A $\beta$  amyloid deposits in the form of diffuse senile plaques (SPs). C) Fluorescence spectra and image (insert) of an A $\beta$  peptide SP and intracellular structures in brain tissue stained with PTAA. PTAA bound to the SPs (yellow-orange) emits red-orange light, which corresponds to the black (squares) fluorescence spectrum. PTAA bound to intracellular structures emits light with a blue color, which corresponds to the blue (triangles) fluorescence spectrum. D) Multifilter fluorescence image of brain tissue containing solid micron-sized plaques emitting red-orange fluorescence (white arrow). The micron-sized plaques were scarce and only present in <5% of this brain section specimen. Images A and B were recorded with an epifluorescence microscope through a 100 $\times$  objective and a 405/30 nm filter (LP450) or a 546/12 nm filter (LP590), respectively. Image C and the spectra were recorded with an epifluorescence microscope through a spectraview module, a 40 $\times$  objective, and a 405/30 nm filter (LP450). Image D is a multifilter image, recorded with an epifluorescence microscope through a 100 $\times$  objective, a 405/30 nm filter (LP450), a 470/40 nm filter (LP515), and a 546/12 nm filter (LP590). The tissue was stained with PTAA (2.5  $\mu\text{g mL}^{-1}$ ) in Na carbonate (100 mM, pH 10) for 2 h. Scale bars (white lines) represent 15  $\mu\text{m}$ .

This tissue specimen also contained other intracellular structures that were stained by PTAA. Importantly, PTAA bound to these different entities fluoresced with a different color (Figure 2A–C). The senile plaques (SPs) showed distinct red cores, whereas the intracellular structures were green, lacking the red component. Moreover, the emission spectra of PTAA bound to SPs or intracellular structures were also significantly different (Figure 2C). Upon binding to the A $\beta$  peptide in the SPs, PTAA adopts a planar conformation, observed as a red-shifted emission spectrum with an emission maximum of 595 nm (Figure 2C). This planarization of the backbone of PTAA has previously been observed for PTAA bound to  $\beta$ -sheet-rich amyloid fibrils of bovine insulin and chicken lysozyme in solution.<sup>[19]</sup> On the other hand, spectra for PTAA bound to intracellular structures are significantly broadened and blue-shifted, with emission maxima of 570 nm (Figure 2C). These blue-shifted spectra resemble the spectrum of PTAA bound to collagen<sup>[19]</sup> and native bovine insulin<sup>[19]</sup> or the spectrum of PTAA in assemblies with a positively charged peptide in which a supramolecular  $\alpha$ -helical structure is formed.<sup>[17]</sup>

Especially, the shoulder at shorter wavelength is associated with twisted and separated polyelectrolyte chains.<sup>[15–20,26]</sup> This indicates different intrinsic structures where the core of the SP is composed of packed  $\beta$ -pleated sheet A $\beta$  peptide and the intracellular structures are composed of more extended structures, probably in a conformation with a helical structure.

To obtain further information on the subcellular localization of the PTAA intracellular structures, brain tissues from an AD patient were co-stained with PTAA and Mayer's nuclear stain, which is specific for positively charged nuclear proteins such as histones. Figure 3E shows a composite multiple-filter fluorescence and transmission image of a serial cut specimen from the same brain tissue as in Figure 3A–D from an AD patient. As discussed above, PTAA binds to vascular amyloid, clearly visible in the heavily stained blood vessels in the lower left part of the image. In this image mode PTAA also show yellow-green fluorescence when bound to intracellular structures, shown with a green arrow. Mayer's reagent specifically stains nuclear proteins and is visible through a

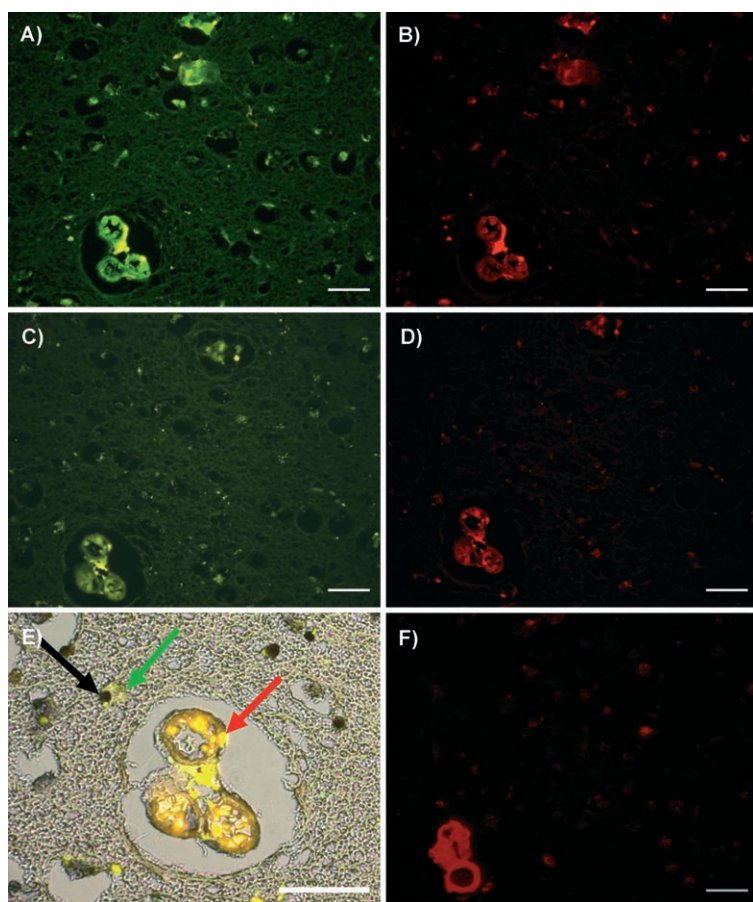


**Figure 3.** Fluorescence images of brain tissue from an AD patient, stained with Mayer's solution, PTAA, and Congo red. A) and B) Tissue stained with PTAA. C), D), and E) Tissue stained with Mayer's reagent and PTAA. F) Tissue stained with Congo red and Mayer's reagent. Images A and C were recorded with an epifluorescence microscope through a 470/40 nm filter (LP450) and a 40 $\times$  objective. Images B, D, and F were recorded with an epifluorescence microscope through a 546/12 nm filter (LP590) and a 40 $\times$  objective. Image E (zoom in region of the vascular vessels seen in the lower left of image C) is a multiframe image recorded with an epifluorescence microscope through a 40 $\times$  objective, a 470/40 nm filter (LP515), and a 546/12 nm filter (LP590) in transmission mode. The red arrow indicates PTAA fluorescence from amyloid-coated vascular vessels, whilst the green arrow indicates fluorescence from intracellular bound PTAA and the black arrow indicates nuclear protein stained with Mayer's reagent. The intracellular structures stained by PTAA are located in the cytoplasm and do not colocalize with the nuclear proteins stained by Mayer's reagent. The tissue was stained with PTAA (2.5  $\mu\text{g mL}^{-1}$ ) in Na carbonate (100 mM, pH 10) for 2 h. Scale bars (white lines) represent 40  $\mu\text{m}$ .

dark brown contrast, which is highlighted with a black arrow (Figure 3E). Although we noted decreased emission intensity from both PTAA and Congo red after staining with Mayer's reagent, these experiments show that PTAA does not colocalize with Mayer's reagent. Mayer's staining results in a blue-black background staining of the samples, which partially absorbs the emitted light from both PTAA and Congo red, so a longer exposure time is needed for the samples stained with Mayer's. From the detailed micrograph (Figure 3E) we can conclude that the partial intracellular staining by PTAA does not colocalize with that of the Mayer's reagent, but that PTAA is instead localized in the cytosol of the same cell in which the Mayer's reagent is staining the nucleus. To determine the biochemical

origin of the intracellular structures stained with PTAA, however, experiments using immunohistological techniques have to be performed; such experiments are in progress but are beyond the scope of this article. Furthermore, experiments correlating normal brain tissue and brain tissue from different stages of the disease are of great interest, as these intracellular structures seem to colocalize with the presence of amyloid and might be usable as progression markers for disease. Such experiments are also in progress.

PTAA was further tested for staining of amyloid light (AL) chain deposits in tissue sections taken from different organs from an AL patient (Figure 4). Interestingly, PTAA emits light of a slightly different color when binding to AL deposits in liver and kidney (Figure 4A and B) or to light chain deposits in a muscle layer in the intestine (Figure 4C). The spectrum (Figure 4D) from PTAA bound to the light chain deposits in the muscle layer in the intestine has a shoulder at shorter wavelengths (550 nm) and the emission maximum (585 nm) is more blue-shifted than the emission maximum (595 nm) seen for PTAA bound to the light chain deposits in the liver and the kidney. The shoulder at shorter wavelengths and the blue shift of the PTAA emission maximum is associated with a more twisted conformation of the polyelectrolyte backbone and separation of polyelectrolyte chains, suggesting that PTAA adopts a more twisted conformation upon interaction with the light chain deposits in the muscle layer in the intestine. This discrepancy could arise from different amounts of serum amyloid P (SAP) component or heparan sulfate proteoglycan (HSPG) decorating the amyloid deposits,<sup>[27]</sup> although PTAA, as mentioned above, is negatively charged at pH 10 and should repel the negatively charged HSPG, so the spectral change is more probably due to differences in the protein conformations within these plaques. As reported previously, deposits in AL disease can be of amyloid fibril type (Congo-phobic) or more diffuse amorphous (Congo negative).<sup>[28–30]</sup> PTAA is a conformation-sensitive probe, so different protein conformations in the deposits might generate geometrical alterations of the polyelectrolyte backbone, affording different emission from the bound PTAA.

Interestingly, similar spectral features (blue shift and emission at 550 nm) have previously been seen for PTAA in complexation with a positively charged peptide forming a helical structure<sup>[17]</sup> and for PTAA bound to native bovine insulin or collagen at pH 7.<sup>[19]</sup> It has been hypothesized that the same protein sequence might give rise to different "strains" of misfolded product in protein aggregation diseases, and our findings might be of great interest for further investigation of this strain phenomenon. It has been shown that the infectivity of different yeast prion strains is dependent on the conformation of the infectious protein, and that a single protein can adopt multiple, self-propagating (infectious) conformations.<sup>[31,32]</sup> The

strain phenomenon might be encoded in the monomer conformation or in the higher-order oligomeric structures of the misfolded protein. In addition, prion strains might also have a major role in determining the specificity of prion transmissibility.<sup>[6,32–34]</sup> It is very tempting to infer that CPs may be usable as optical probes for discrimination of different strains of amyloidogenic proteins. More work with different amyloidogenic proteins, including more AL tissue samples, will have to be performed to validate the results observed for the light chain deposits in this study; such experiments, with a variety of different proteins, are ongoing in our laboratories.

The use of PTAA as an amyloid-specific dye was further demonstrated with two-photon excitation (TPE) fluorescence, as there is clinical importance in imaging amyloid deposits in vivo. Probes for fluorescence imaging of amyloid plaques by multiphoton microscopy have been reported previously, and this technique might be valuable for early diagnosis and monitoring of disease progression of amyloidoses, especially Alzheimer's disease.<sup>[35–39]</sup> Multiphoton microscopy uses long-wavelength light to excite the fluorophore, and one advantage of multiphoton excitation is that the excitation occurs only in the very small focal point volume of the objective lens that focuses the laser.<sup>[40]</sup> It is also possible to obtain images of microscopic structures several hundred micrometers below the surface of the brain in a living animal by the use of multiphoton microscopy, since the NIR wavelengths often used (typically 700–900 nm) have relatively good transmission in living tissue, in relation to wavelengths in the UV or in the visible region.

As shown in Figure 5, A $\beta$  peptide SP deposition in brain tissue sections can be visualized by the red emission from PTAA upon multiphoton excitation at 820 nm. The amyloid deposit can easily be distinguished from the rest of the tissue, providing imaging of amyloid deposits with high sensitivity and superior contrast between the signals from the amyloid deposits and the surrounding tissue. Moreover, we noted that the emission spectrum of PTAA in the case of multiphoton excitation of SP deposition is usually more red-shifted (peak at approximately 620 nm) than the spectrum observed by single-photon excitation (peak at 595 nm). This could be explained by a difference in sensitivity between PTAA conformations that

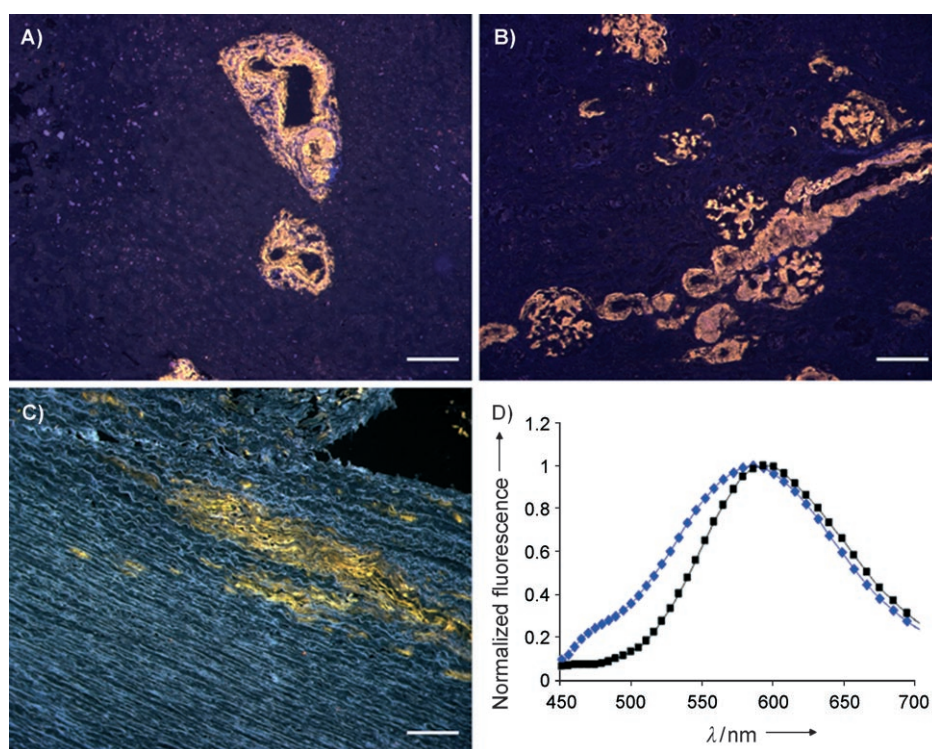


**Figure 4.** Fluorescence images and spectra of AL amyloid stained with PTAA (formaldehyde-fixed, paraffin-embedded tissue samples). A) Liver tissue containing AL amyloid. B) Kidney tissue containing AL amyloid. C) Muscle layer in intestine containing AL amyloid. PTAA bound to amyloid in liver and kidney (orange-red) emits orange-red light, which corresponds to the black (squares) fluorescence spectrum (D). PTAA-bound amyloid in the muscle layer (yellow) emits light with a green-yellow color, which corresponds to the blue (diamonds) fluorescence spectrum. Images A–C are multifilter images recorded with an epifluorescence microscope through a 10 $\times$  objective, a 405/30 nm filter (LP450), a 470/40 nm filter (LP515), and a 546/12 nm filter (LP590). The spectra were recorded with an epifluorescence microscope fitted with a spectraview module, through a 10 $\times$  objective and a 405/30 nm filter (LP450). The tissues were stained with PTAA (2.5  $\mu\text{g mL}^{-1}$ ) in Na carbonate (100 mM, pH 10) for 2 h. Scale bars (white lines) represent 150  $\mu\text{m}$ .

are planar—possessing a strong two-photon absorption (TPA) cross-section—and nonplanar ones. Planar conformations also give more pronounced red shifts and have higher quantum yields than the nonplanar conformations. A previous study of POMT and related analogues to PTAA at different pH values showed TPAs and quantum efficiencies two to four times stronger when the backbones of the CPs adopt planar conformations and the polyelectrolytes chains were separated.<sup>[25]</sup> As a result, the TPE process is more selective with regard to planar conjugated structures. In this context it was interesting to note that the PTAA bound to the intracellular structures in the very same sample was not emitting light under TPE; this implies that the conformations of PTAA binding to intracellular structures and to SPs are considerably different. Further work to investigate details of polarization and spectral features with the aid of PTAA and related conjugated polyelectrolytes in TPE imaging of amyloid deposits and protein conformations are in progress. Syntheses of novel polythiophene derivatives that will function as amyloid-specific dyes under physiological conditions are also in progress, as such probes are required for in vivo experiments. Furthermore, the ideal situation would also be to have probes that emit light in the 700 to 900 nm range for carrying out in vivo imaging. However, it is well known that

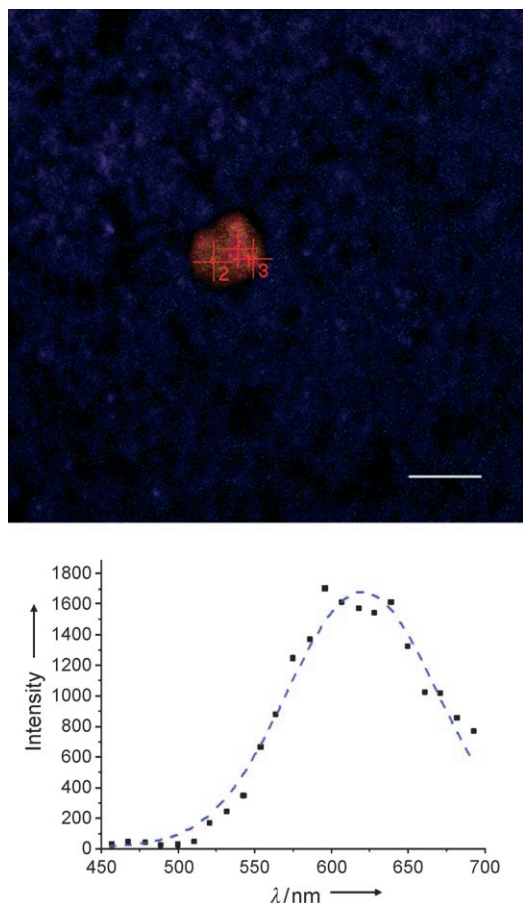


**Figure 5.** TPE image (top) and spectra (bottom) of amyloid-containing formaldehyde-fixed, paraffin-embedded AD brain tissue stained with PTAA. The SPs emit red light and are easily distinguished from the surrounding tissue (black/blue). The spectrum (black squares) shows a peak at approximately 620 nm and was calculated as an average from data points (see Figure S1 in the Supporting Information) taken from three independent spectral pixels (labeled in the image) and fitted to a Gaussian function (dashed blue line). The image and the spectra were recorded on an LSM 510 META (Carl Zeiss, Jena, Germany) confocal laser scanning microscope with a Plan-Neofluar 40 $\times$ /0.75 objective. The sample was excited with a laser tuned to 820 nm and the emitted fluorescence was detected by a photomultiplier tube array detector with 32 elements (META detector accessory). The tissue was stained with PTAA (2.5  $\mu\text{g mL}^{-1}$ ) in Na carbonate (100 mM, pH 10) for 2 h. Scale bar (white line) represents 40  $\mu\text{m}$ .

the critical element in TPE is that the laser-spot should have a well defined focus. TPE imaging uses no aperture in front of the detector, as in the case of confocal microscopy, since the focal volume itself, along with the nonlinear absorption (makes spot even smaller), defines the resolved excitation volume. Here, the aperture in front of the detector is completely open in order to collect as much light as possible, so scattered emitted light is also collected, which decreases the demand for "complete transparency" for the visible wavelengths.

## Conclusion

This is the first study on the binding properties of CPs to amyloid fibril deposits present in different human tissues. Previous studies<sup>[19,20]</sup> have shown that PTAA and PONT can be used to

detect amyloid-like fibril formation by isolated proteins in solution. It is apparent that CP probes can report conformational differences in proteins and thus might offer improvements in specificity over the small-molecule dyes commonly used today, as these probes only change their optical features as a function of whether they are free in solution or bound to a protein. In this study, we have shown that CP probes can be used as amyloid-specific dyes. Furthermore, the variation in the fluorescence from PTAA bound to light chain deposits in different organs could possibly depend on altered conformations in the backbones of the PTAA molecule caused by different conformations of the protein in the AL deposits, so CP probes might possibly offer a novel approach to discriminating between amyloid fibrils with different conformations. In this regard, conformation-sensitive CP probes might facilitate a greater understanding of the conformational phenotypes encoded in different prion strains, and conformation-selective probes of this type could have a considerable impact on the diagnoses of diseases associated with misfolded proteins and protein aggregates. Currently, early-stage therapeutic interventions into the misfolding diseases are limited by the absence of sensitive diagnostic tests for the culprit misfolded protein. Our future efforts with this technique will be to evaluate the methodology and to correlate it against other standard staining methods used in the study of amyloidoses and other related diseases. We foresee that the use of CPs as conformation-sensitive probes might be a powerful addition to the standard techniques for studying protein misfolding processes and for evaluating pathological changes in amyloidoses.

## Experimental Section

The syntheses of the conjugated polyelectrolytes have been reported elsewhere.<sup>[20,25,41]</sup> Amyloid-containing tissues were kindly provided by Prof. Per Westermark, Department of Genetics and Pathology, Uppsala University, Uppsala, Sweden. These tissues were decoded and approved for research.

Frozen sections from pancreas were fixed in ice-cold acetone or ethanol for 10 min and washed with Tris-HCl (0.05 M, pH 7.4) containing NaCl (0.15 M). The sections were equilibrated in incubation buffer solutions, Na carbonate (100 mM, pH 10) or glycine-HCl (100 mM, pH 2.5), for 10 min. PTAA and PONT (1.0 mg mL<sup>-1</sup> in deionized water) were diluted with Na carbonate (100 mM, pH 10; 0.25  $\mu\text{g}$  probe in 100  $\mu\text{L}$ ) and added to the sections. PONT (1.0 mg mL<sup>-1</sup> in deionized water) was diluted in glycine-HCl (100 mM, pH 2.5; 0.25  $\mu\text{g}$  probe in 100  $\mu\text{L}$ ) and added to the sections equilibrated with the same glycine buffer. The incubation was carried out in a humidity chamber for 2 h at room temperature and superfluous probe solution was washed away with incubation buffer. The fluorescence from the tissue samples was recorded with an epifluorescence microscope (Zeiss Axiovert A200 Mot inverted microscope) fitted with a CCD camera (Axiocam HR), through a 405/30 nm bandpass filter (LP450), a 470/40 nm bandpass filter (LP515), and a 546/12 nm bandpass filter (LP590). Each of the polyelectrolytes was tested on 10 different sections ( $N=10$ ).

Sections (5  $\mu\text{m}$ ) from formaldehyde-fixed, paraffin-embedded amyloid-containing tissue were placed on plus-slides (Histolab, Göteborg, Sweden) and deparaffinized with xylene (2 $\times$ 30 min), absolute alcohol (2 $\times$ 10 min), 95% alcohol (10 min), and 70% alcohol

(10 min) and finally rinsed in distilled water. The sections were equilibrated in incubation buffer solution (Na carbonate, 100 mM, pH 10) for 10 min. PTAA (1.0 mg mL<sup>-1</sup> in deionized water) was diluted with the same buffer as used for equilibration (0.25 µg probe in 100 µL) and added to the sections. The incubation was carried out in a humidity chamber for 2 h at room temperature and superfluous probe solution was washed away with incubation buffer. Cell nuclei were stained with Mayer's nuclear stain (0.1% hematoxylin, 5% chloral hydrate, 5% ammonium alum, and 0.02% sodium iodate in water) for 2 min, followed by continuous rinsing in tap water for 10 min. The fluorescence from the tissues samples were recorded as above. The spectra from PTAA in the tissue samples were recorded with the same setup, fitted with a Spectravis™ 1.6 (Applied Spectral Imaging, Migdal Ha'emek, Israel) and a Spectra-Cube® (Optical head) module, through a 405/30 nm bandpass filter (LP450). The data were processed with Spectral Imaging 2.6. PTAA was tested on samples from more than five cases of AL and the staining was performed on sections (N=5) from different tissue of these cases. Furthermore, PTAA was tested on three cases of AD and the staining was performed on brain sections (N=5) from these cases.

Congo red staining was performed as described by Puchtler et al.<sup>[22]</sup> Paraffin sections were deparaffinized prior to Congo red staining. The nuclei were counterstained in Mayer's hematoxylin solutions for 1 min and then rinsed in tap water. Congo red staining was performed in solution A (saturated solution of sodium chloride in 80% ethanol with 0.01% NaOH) for 20 min, and the sections were then transferred directly to solution B (sodium chloride-saturated 80% ethanol solution with 0.2 g L<sup>-1</sup> Congo red and 0.01% NaOH) and incubated for another 20 min. The fluorescence from the tissues samples were recorded as described above.

Two-photon excitation (TPE) fluorescence imaging was performed with an LSM 510 META (Carl Zeiss, Jena, Germany) confocal laser scanning microscope through Plan-Neofluar 10×/0.3, 20×/0.5, and 40×/0.75 objectives. A Mira Model 900-F mode-locked Ti:sapphire laser (Coherent, Inc., Santa Clara, CA) was pumped with a solid-state Verdi V-5 laser operating at 532 nm (Coherent, Inc.). The laser produced 200 fs pulses at a repetition rate of 76 MHz with an average output power of 750 mW from the laser cavity, and approximately 20–40 mW at the objective for λ = 820 nm. Typically, 15–50% of this power was needed for image recording by TPE fluorescence as discussed in the text. With the laser tuned to 830 nm, samples were excited and the emitted fluorescence were detected with a photomultiplier tube array detector with 32 elements capable of detecting emission light between 377 and 719.4 nm in steps of 10.7 nm (META detector accessory). The presentation of images and selection of spectral regions was achieved with the standard software.

## Acknowledgements

We thank professor Per Westermark for providing amyloid-containing tissue samples. This work was partially funded by VINNOVA (A.H.), CENANO (Linköping University), a grant from the Norwegian Research Council within the NanoMat program (Contract #153529s10; M.L.), the Swedish Nanotek program (P.H. and M.L.), Novo Nordisk fund (G.W.), and the Swedish Diabetes association (G.W.). Support from the Swedish foundation for strategic research (SSF; P.H.), the Wenner-Gren foundations (P.H.), and the Swedish Research Council (P.H. and G.W.) is greatly appreciated.

**Keywords:** amyloid deposits • conformation • conjugated polyelectrolytes • fluorescent probes

- [1] R. W. Carrell, D. A. Lomas, *Lancet* **1997**, *350*, 134–138.
- [2] S. B. Prusiner, *Science* **1997**, *278*, 245–251.
- [3] S. B. Prusiner, *Proc. Natl. Acad. Sci. USA* **1998**, *95*, 13363–13383.
- [4] F. E. Cohen, S. B. Prusiner, *Annu. Rev. Biochem.* **1998**, *67*, 793–819.
- [5] C. Govaerts, H. Wille, S. B. Prusiner, F. E. Cohen, *Proc. Natl. Acad. Sci. USA* **2004**, *101*, 8342–8347.
- [6] G. Legname, I. V. Baskakov, H. O. Nguyen, D. Riesner, F. E. Cohen, S. J. DeArmond, S. B. Prusiner, *Science* **2004**, *305*, 673–676.
- [7] E. D. Eanes, G. G. Glenner, *J. Histochem. Cytochem.* **1968**, *16*, 673–677.
- [8] M. Sunde, L. C. Serpell, M. Bartlam, P. E. Fraser, M. B. Pepys, C. C. Blake, *J. Mol. Biol.* **1997**, *273*, 729–739.
- [9] C. M. Dobson, *Trends Biochem. Sci.* **1999**, *24*, 329–332.
- [10] P. Hammarström, X. Jiang, A. R. Hurshman, E. T. Powers, J. W. Kelly, *Proc. Natl. Acad. Sci. USA* **2002**, *99*, 16427–16432.
- [11] M. R. Krebs, C. E. Macphee, A. F. Miller, I. E. Dunlop, C. M. Dobson, A. M. Donald, *Proc. Natl. Acad. Sci. USA* **2004**, *101*, 14420–14424.
- [12] J. D. Harper, S. S. Wong, C. M. Lieber, P. T. Lansbury, *Chem. Biol.* **1997**, *4*, 119–125.
- [13] J. D. Harper, P. T. Lansbury, *Annu. Rev. Biochem.* **1997**, *66*, 385–407.
- [14] G. T. Westermark, K. H. Johnson, P. Westermark, *Methods Enzymol.* **1999**, *309*, 3–25.
- [15] K. P. R. Nilsson, O. Inganas, *Nat. Mater.* **2003**, *2*, 419–424.
- [16] K. P. R. Nilsson, J. Rydberg, L. Baltzer, O. Inganas, *Proc. Natl. Acad. Sci. USA* **2003**, *100*, 10170–10174.
- [17] K. P. R. Nilsson, J. Rydberg, L. Baltzer, O. Inganas, *Proc. Natl. Acad. Sci. USA* **2004**, *101*, 11197–11202.
- [18] K. P. R. Nilsson, O. Inganäs, *Macromolecules* **2004**, *37*, 9109–9113.
- [19] K. P. R. Nilsson, A. Herland, P. Hammarström, O. Inganäs, *Biochemistry* **2005**, *44*, 3718–3724.
- [20] A. Herland, K. P. R. Nilsson, J. D. M. Olsson, P. Konradsson, P. Hammarström, O. Inganäs, *J. Am. Chem. Soc.* **2005**, *127*, 2317–2323.
- [21] H. Puchtler, F. Sweat, M. Levine, *J. Histochem. Cytochem.* **1962**, *10*, 355–364.
- [22] H. Puchtler, F. Sweat, *J. Histochem. Cytochem.* **1965**, *13*, 693–694.
- [23] T. Kitamoto, K. Ogomori, J. Tateishi, S. B. Prusiner, *Lab. Invest.* **1987**, *57*, 230–236.
- [24] S. D. Styren, R. L. Hamilton, G. C. Styren, W. E. Klunk, *J. Histochem. Cytochem.* **2000**, *48*, 1223–1232.
- [25] K. P. R. Nilsson, J. D. M. Olsson, F. Stabo-Eeg, M. Lindgren, P. Konradsson, O. Inganäs, *Macromolecules* **2005**, *38*, 6813–6821.
- [26] K. P. R. Nilsson, M. R. Andersson, O. Inganäs, *J. Phys. Condens. Matter* **2002**, *14*, 10011–10020.
- [27] J. D. Sipe, A. S. Cohen, *J. Struct. Biol.* **2000**, *130*, 88–98.
- [28] G. Gallo, M. Picken, B. Frangione, J. Buxbaum, *Mod. Pathol.* **1988**, *1*, 453–456.
- [29] B. Kaplan, R. Vidal, A. Kumar, J. Ghiso, B. Frangione, G. Gallo, *Clin. Exp. Immunol.* **1997**, *110*, 472–478.
- [30] M. B. Stokes, J. Jagirdar, O. Burchstin, S. Kornacki, A. Kumar, G. Gallo, *Mod. Pathol.* **1997**, *10*, 1059–1065.
- [31] M. Tanaka, P. Chien, N. Naber, R. Cooke, J. S. Weissman, *Nature* **2004**, *428*, 323–328.
- [32] G. Legname, H-O. B. Nguyen, I. V. Baskakov, F. E. Cohen, S. J. DeArmond, S. B. Prusiner, *Proc. Natl. Acad. Sci. USA* **2005**, *102*, 2168–2173.
- [33] P. Chien, J. S. Weissman, *Nature* **2001**, *410*, 223–227.
- [34] P. Chien, A. H. DePace, S. Collins, J. S. Weissman, *Nature* **2003**, *424*, 948–951.
- [35] B. J. Bacskai, S. T. Kajdasz, R. H. Christie, C. Carter, D. Games, P. Seubert, D. Schenk, B. T. Hyman, *Nat. Med.* **2001**, *7*, 369–372.
- [36] W. E. Klunk, B. J. Bacskai, C. A. Mathis, S. T. Kajdasz, M. E. McLellan, M. P. Frosch, M. L. Debnath, D. P. Holt, Y. Wang, B. T. Hyman, *J. Neuropathol. Exp. Neurol.* **2002**, *61*, 797–805.
- [37] B. J. Bacskai, G. A. Hickey, J. Skoch, S. T. Kajdasz, Y. Wang, G-F. Huang, C. A. Mathis, W. E. Klunk, B. T. Hyman, *Proc. Natl. Acad. Sci. USA* **2003**, *100*, 12462–12467.
- [38] S. D. Styren, R. L. Hamilton, G. C. Styren, W. E. Klunk, *J. Histochem. Cytochem.* **2000**, *48*, 1223–1232.

- [39] E. E. Nesterov, J. Skoch, B. T. Hyman, W. E. Klunk, B. J. Bacskai, T. M. Swager, *Angew. Chem.* **2005**, *117*, 5588–5592; *Angew. Chem. Int. Ed.* **2005**, *44*, 5452–5456.
- [40] W. Denk, J. H. Strickler, W. W. Webb, *Science* **1990**, *248*, 73–76.
- [41] L. Ding, M. Jonforsen, L. S. Roman, M. R. Andersson, O. Inganäs, *Synth. Met.* **2000**, *110*, 133–140.

---

Received: December 21, 2005  
Published online on May 26, 2006